Technology in Cancer Research & Treatment
ISSN 1533-0346
Volume 4, Number 4, August (2005)

Spectral Polarization Imaging of Human Prostate Cancer Tissue Using a Near-infrared Receptor-targeted Contrast Agent

www.tcrt.org

Y. Pu, B.S.[1]
W. B. Wang, Ph.D.[2]
G. C. Tang, M.S.[2]
F. Zeng, B.S.[2]
S. Achilefu, Ph.D.[3]
J. H. Vitenson, M.D.[4]
I. Sawczuk, M.D.[6]
S. Peters, M.D.[5]
J. M. Lombardo, M.D.[5]
R. R. Alfano, Ph.D.[2,*]

[1]Department of Electrical Engineering
[2]Department of Physics
The City College of the City Univ. of NY
Convent Avenue at 138th Street
New York, NY 10031
[3]Washington University School of Medicine
4525 Scott Avenue
St. Louis. Missouri 63110
[4]Department of Urology
[5]Department of Pathology
Hackensack University Medical Center
30 Prospect Avenue
Hackensack, NJ 07601
[6]Department of Urology
Hackensack University Medical Center
Adjunct Professor of Urology
College of Physicians and Surgeons
Columbia University
Professor of Surgery (Urology)
UMDNJ Newark Medical School

* Corresponding Author:
R. R. Alfano, Ph.D.
Email: alfano@sci.ccny.cuny.edu

The Cypate-Bombesin Peptide Analogue Conjugate (Cybesin) was used as a prostate tumor receptor-targeted contrast agent. The absorption and fluorescence spectra of Cybesin were measured and shown to exist in the NIR tissue "optical window". The spectral polarization imaging of Cybesin-stained prostate cancerous and normal tissues shows that prostate cancerous tissue takes-up more Cybesin than that of prostate normal tissue, making Cybesin a potential marker of prostate cancer.

Keywords: Prostate cancer; Receptor-targeted; Peptide analogue conjugate; Contrast agent; Spectral polarization imaging; Near-infrared; Absorption; and Fluorescence.

Introduction

The increasing incidence and mortality rate of prostate cancers in men makes early tumor detection research a challenge for oncological specialists. The region of the highest incidence is in the western world, where there are 10-11% chances for a man to develop prostate cancer, and 3-4% chances of dying from the disease (1). Conventional oncology imaging methods for prostate cancer diagnosis, still depend on bulk physical properties of cancer tissue and are not effective for early-stage primary tumors (2). It is well known that diagnosis of a small premalignant lesion is critical for the success of cancer therapy and a key to increase survival rates. Scientists have been looking for methods that emphasize gene-specific or receptor-specific, minimally invasive diagnosis for early-stage tumors (2).

Near-infrared (NIR) optical imaging is a powerful tool in cancer research that relies on activating endogenous chromophores or applying contrast agents that can target cancer cells. The use of intrinsic chromophores to differentiate the optical properties of diseased and healthy human tissues has been reported in some studies using fluorescence and absorption (3, 4). The most attractive advantage of optical imaging is the high sensitivity, which can be superior to other *in vivo* imaging techniques (2). Over the past decade, cyanine dyes have been investigated by several groups (5, 6) as contrast agents for optical detection of tumors. In order to observe fluorescence from a substantial distance within the body, the emission wavelength must be in the NIR wavelength window in which light passing through tissue is less likely to be absorbed or scattered (7). Researchers are interested in cyanine dyes because their emission range of 700 nm to 900 nm is in the tissue "optical window" (8). Indocyanine Green (ICG, also called cardio-green), a clinically approved NIR dye by FDA, is one of the most investigated cyanine dyes. Its fluorescence range is between 775 nm and 850 nm, that avoids the

absorption bands at 950nm and 1195nm due to water which is the main chromophore component in human tissue (4, 9).

The investigations of receptor expression in normal and cancer tissue suggest that small peptide-dye conjugates can be used to target over-expressed receptors on tumors contrary to the traditional approach of dyes conjugated to large proteins and antibodies (5, 10, 11). As a small ICG-derivative dye-peptide, Cypate-Bombesin Peptide Analogue Conjugate (Cybesin) was synthesized and used as a contrast agent to detect pancreas tumors in an animal model a few years ago (5). The prior experimental results of Cybesin for tumor detection indicated that Cybesin preferentially localized for over 24 hours in tumors known to over-express bombesin receptors in a small animal model (5). In this study, Cybesin was used to target over-expressed bombesin receptors in human prostate cancer tissue. Bombesin belongs to a family of brain-gut peptides that play an important role in cancer development (12). It was observed that human primary tumors can synthesize bombesin (12), and the bombesin receptor can also be over-expressed on the membranes of human prostate cancer cells (12). All of these results motivated us to apply Cybesin to human prostate cancer detection.

In this paper, we report our NIR spectral polarization imaging study using Cybesin as an optical contrast agent marker to differentiate human prostate cancerous and normal tissues. The absorption and fluorescence spectra of Cybesin were studied in the wavelength region from 650 nm to 900 nm. The model prostate samples consisting of a small piece of normal prostate tissue and a small piece of prostate cancer tissues stained with Cybesin were imaged. The results indicate that this receptor-targeted Cybesin was preferentially taken up by prostate cancerous tissue compared to prostate normal tissues.

Materials and Methods

Experimental Method and Sample

The schematic diagram of the experimental set-up for our NIR spectral polarization imaging is shown in Figure 1. Light from a white light source is used to illuminate the prostate tissue sample with average power of about 50 $\mu W/cm^2$, which is much lower than the critical illumination level given by FDA. The illumination wavelengths are selected by wide-band pass filters varying from 550 nm to 900 nm with FWHM=40 nm placed on a multiple filter wheel, which can be rotated to the desired filter position by computer control. A CCD camera records images formed by light emitted from the sample. The detection wavelength is selected by rotating a similar set of band pass filters placed on the second multiple filter wheel located in front of the detector. Polarizer P_1 used to ensure linear polarization of the illumination and polarizer P_2 is placed in the front of the CCD for selecting the detection polarization. Images are recorded when the detection polarization is parallel or perpendicular to the illumination polarization (7). For emission light imaging, the wavelengths of the band pass range of the detection (imaging) filter is longer than that of the illumination so that the pump light is blocked, and only the light emitted from the sample is collected by the CCD camera (7).

Eight [8] *in vitro* prostate cancer-and-normal tissue samples obtained from Hackensack University Medical Center (HUMC) and the National Disease Research Interchange (NDRI) were used for optical imaging measurements. The results of histological section measurements performed at the Pathology Department of HUMC were used as a guide to indicate the locations of the cancerous and normal tissue areas. The prostate normal tissues were cut into a number of large slices with thicknesses of 1.0 mm to 4.5 mm and used as host tissue. The experiments were performed under IRB approvals at HUMC and CCNY (City College of New York).

A typical prostate cancerous-normal tissue sample used for the imaging measurements consists of a small piece of prostate cancer tissue and a small piece of prostate normal tissue. Both of them have a similar size and were soaked in the same Cybesin-DMSO (in 20% aqueous Dimethyl Sulfoxide) solution with a Cybesin concentration of ~3.2×10^{-6} M for the same period of time. Then the samples were put into sodium phosphate buffer (Sigma-Aldrich) to wash off the unbound Cybesin. The stained normal and cancer tissues were then sandwiched between large pieces of prostate normal tissue. The depth of the stained tissue underneath the surface of the host prostate normal tissue was varied to obtain the detectable imaging depths. The schematic diagram of a sandwiched prostate cancerous-and-normal tissue sample is shown at the sample position in Figure 1.

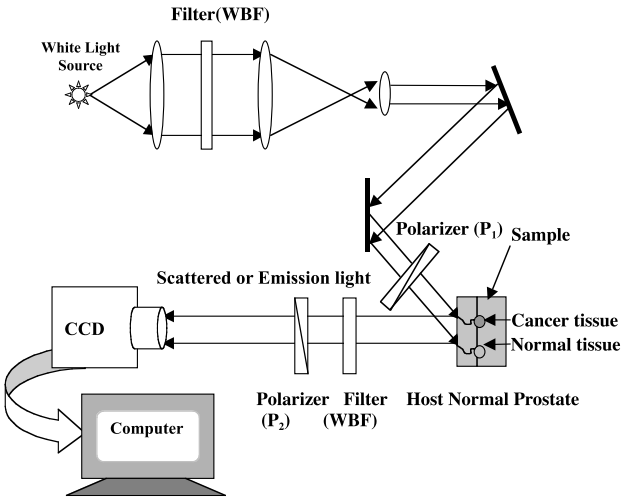

Figure 1: Schematic diagram of our spectral polarization imaging set-up. The structure of a sandwiched prostate cancerous-and-normal tissue sample is schematically shown in the sample position.

The prostate tissue from which the stained normal and cancerous tissue pieces were taken was cut into a number of slides with a thickness of 250 μm at HUMC for microscopy study. The microscope images were taken using a digital electromicroscope (Mel Sobel Microscopes Ltd) and compared with the results obtained from the optical imaging. Figures 2(a) and (b) show the low power (×40) microscope images of the normal and cancerous areas of prostate tissue, respectively.

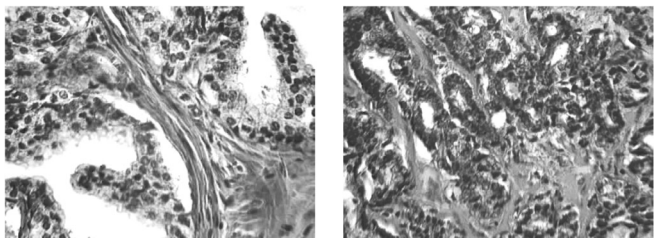

Figure 2: (**a**) 40 times magnified microscope image of the normal area in a prostate tissue sample and (**b**) 40 times magnified microscope image of the cancerous area in a prostate tissue sample. The cancer is estimated as Gleason grade 3+4.

The Absorption and Fluorescence Spectra of Cybesin

Cybesin was prepared by Achilefu's group at the Washington University School of Medicine. The molecular structure of Cybesin is shown in Figure 3. It is mainly composed of ICG and the bombesin receptor ligand, which delivers the ICG to the receptor presented in the tumor (5). The synthesis of this contrast agent was reported elsewhere (5). The previous investigation shows that Cybesin can be used for effectively targeting a bombesin-rich tumor in the animal model because of the high affinity of Cybesin for the bombesin receptor (5). The schematic for Cybesin targeting the bombesin receptor on a tumor is also shown in Figure 3.

In this study, we investigated the over-expressed bombesin receptor status in human prostate cancer cells. A variety of tumor tissues have been found to express bombesin receptors, for instance prostate, lung, breast, and pancreas tumors

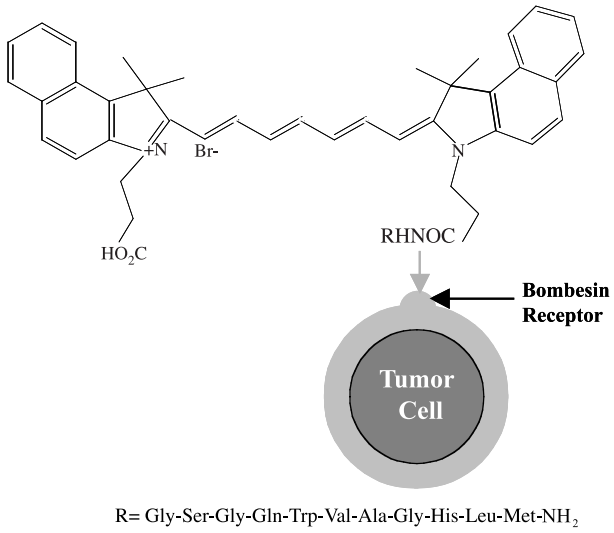

Figure 3: Molecular structure of the Cypate-Bombesin Peptide Analogue Conjugate (Cybesin), and schematic diagram of Cybesin targeting to the bombesin receptor on prostate tumor cells.

(12, 13). The optical imaging for human prostate cancer detection using this contrast agent depends on the two factors: (i) The high affinity of Cybesin for the bombesin receptor (5) and (ii) the over-expressed bombesin receptor status of human prostate cancer cells (12, 13).

In our study, Cybesin was solvated in 20% aqueous Dimethyl Sulfoxide (DMSO). The absorption spectrum of Cybesin in DMSO solution was investigated using a Perkin-Elmer Lamda 9 UV/VIS/NIR Spectrophotometer in the spectral range of 300 nm to 900 nm. The fluorescence spectrum was measured using a far-red to NIR spectral setup excited by modulated excitation with a 680 nm diode laser. Fluorescence light from the sample after passing through lenses was focused on the entrance slit of a SPEX Minimate 0.25-m monochromator (spectrometer) and detected by a Hamamatsu P394A PbS detector mounted at the exit slit of the monochromator. Signals from the detector were recorded by a PAR Model HR-8 lock-in amplifier connected to a computer.

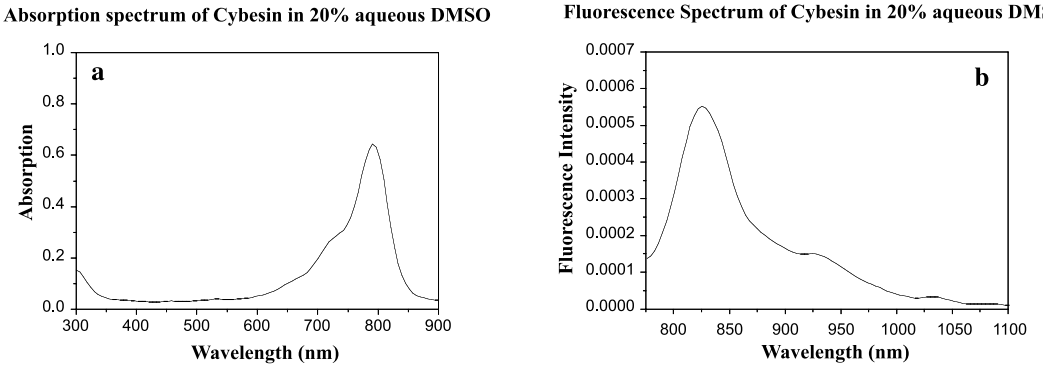

Figure 4: (**a**) Absorption and (**b**) fluorescence spectra of Cybesin in 20% aqueous DMSO. The fluorescence was excited by a 680 nm diode laser.

Figure 4(a) and (b) show the measured absorption and fluorescence spectra of Cybesin, respectively. The absorption band of Cybesin ranges from 680 nm to 830 nm with a shoulder peak at 720 nm and a strong peak at 792 nm. The fluorescence spectrum covers from 800 nm to 950 nm with a main peak at 825 nm and a weak peak at 925 nm. Both results show that Cybesin possesses the spectral advantages of ICG that the fluorescence and the absorption ranges are in the NIR range of the "tissue optical window".

Optical Imaging Result and Discussion

In order to investigate the affinity of Cybesin for prostate cancer tissue and obtain the optimal spectral imaging conditions, the samples were imaged at different wavelengths, polarizations, and depths in which the stained small pieces of the cancerous and normal tissues were embedded inside the host prostate tissue.

The contrast agent emission images of the samples were recorded at different pump and detection wavelengths varying from 650 nm to 850 nm. In order to compare images recorded at different wavelengths in the same polarization configuration, the perpendicular images were recorded. Figure 5 shows perpendicular polarization images of stained cancerous and normal prostate tissue on the host normal prostate tissue recorded at different detection wavelengths of 750 nm to 850 nm. The salient features shown in Figure 5

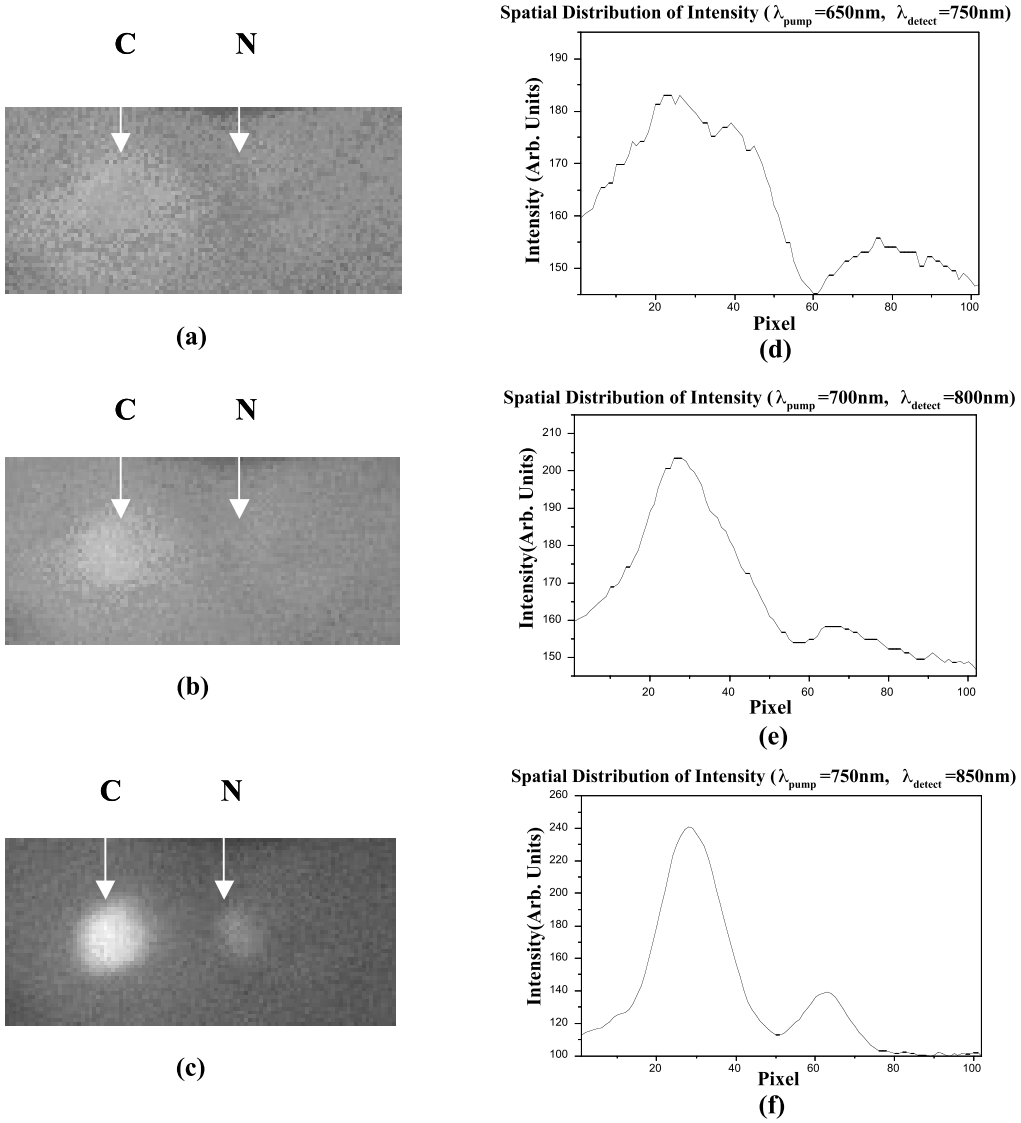

Figure 5: Contrast agent emission images of a prostate cancer-and-normal tissue sample recorded at (**a**) λ_{pump}=650nm and $\lambda_{detection}$=750nm, (**b**) λ_{pump}=700nm and $\lambda_{detection}$=800nm, and (**c**) λ_{pump}=750nm and $\lambda_{detection}$=850nm, with a perpendicular polarization configuration; (**d**), (**e**), and (**f**) are the cross section intensity distributions of the images of (**a**), (**b**), and (**c**) at the same row crossing the areas of the stained cancer (C) and normal (N) tissues, respectively. The intensity in the cancerous tissue area is much greater than that of the normal tissue area.

is that the dyed small pieces of cancer and normal tissues can not be clearly distinguished from the image acquired with short pump and detection wavelengths at λ_{pump}=650 nm and $\lambda_{detection}$=750 nm, while the tumor can be recognized by the images obtained with longer pump and detection wavelengths at λ_{pump}=750 nm and $\lambda_{detection}$=850 nm. When the wavelength increases, the visibility of the dyed object increases dramatically. The measured results show that the optimized detection wavelength range is from 800 nm to 850 nm, which is exactly the strong fluorescence range of Cybesin. This indicates that the recorded images are indeed formed from the contrast agent emission, not from the tissue's native emission. It can be seen from the images that the cancerous tissue piece is much brighter than that of the normal tissue piece indicating that the prostate cancer tissues adsorb Cybesin more than normal tissues because Cybesin targets the over-expressed bombesin receptors of human prostate cancer cells (12, 13). On the other hand, since malignant tumors are more cell-packed (14), there will be more cells in cancerous area, even for same size, geometry, or weight, and hence more, Cybesin binds to cancerous area versus normal area. We believe that both high adsorption and density of cancer cells contribute to the large fluorescence intensity in the cancerous area, and make Cybesin a good candidate as a marker to differentiate prostate cancerous tissue from the normal tissue.

The difference between cancerous and normal tissue images can be more clearly seen from their spatial intensity distributions at the same pixel row crossing the areas of the stained cancer and normal tissues. Figures 5(d), (e), and (f) show the digital spatial cross section intensity distributions of the images shown in Figures 5(a), (b), and (c), respectively. The image obtained at λ_{pump}=750 nm and $\lambda_{detection}$=850 nm shows the best visibility and greatest difference between normal and cancerous tissue. Under this best imaging condition, the ratio of imaging intensity of cancerous tissue area to that of normal tissue area is found to be ~3.55.

As described in our previous study (15, 16), the polarization preservation property of ICG and the fluorescence polarization difference imaging technique can be used to improve the image quality of a fluorescent object embedded in tissues. In order to determine if Cybesin has a polarization preservation property, we studied Cybesin emission images recorded at different polarization configurations. The polarization dependence of fluorescence images of the stained cancerous and normal prostate tissue surrounded by the host normal prostate tissue at λ_{pump}=750 nm and $\lambda_{detection}$=850 nm is shown in Figure 6. Figure 6(a) displays the parallel image recorded

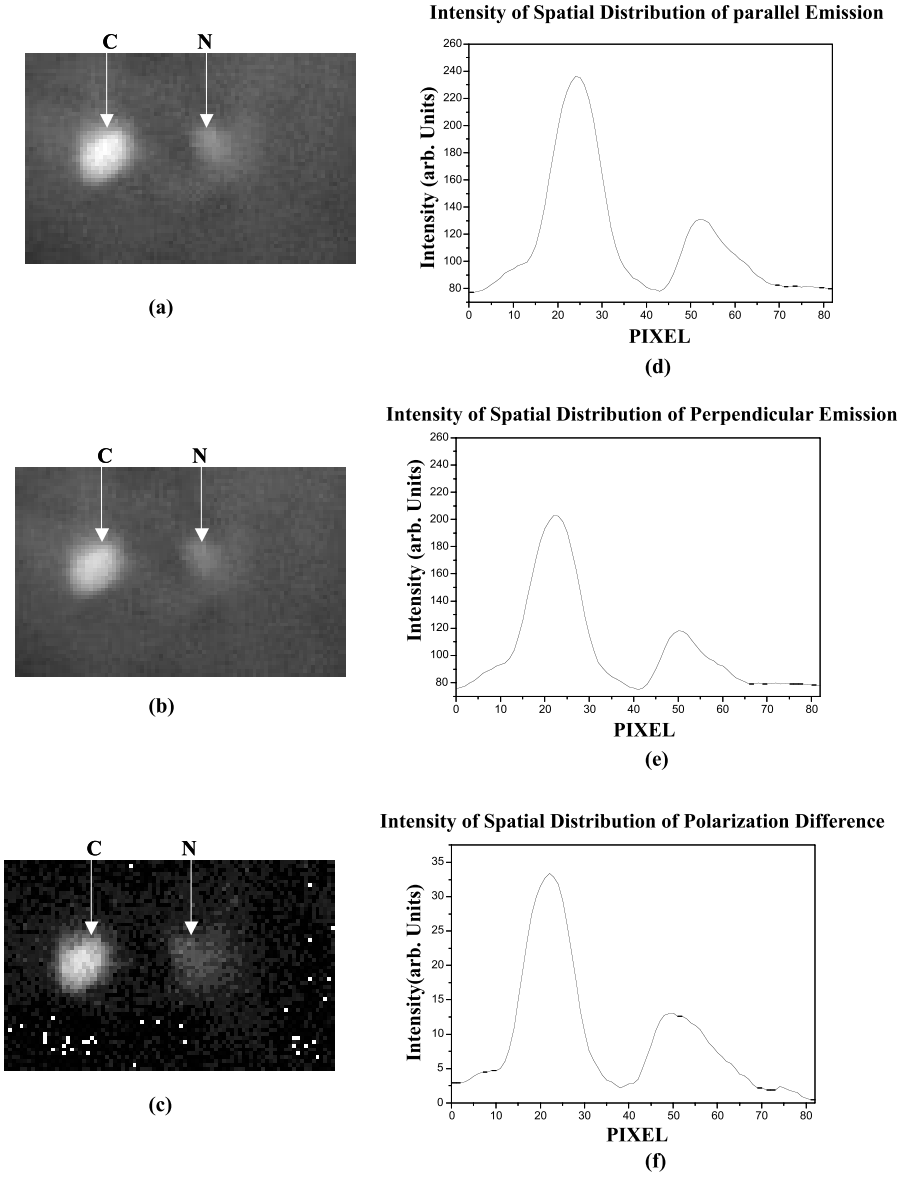

Figure 6: Polarization dependence of fluorescence images of a cancerous and normal prostate tissue sample recorded at λ_{pump}=750nm and $\lambda_{detection}$=850nm when the polarization direction of P_2 is parallel (**a**) and perpendicular (**b**) to that of the illuminating light. (**c**) is the polarization difference image obtained by subtracting (**b**) from (**a**). (**d**), (**e**), and (**f**) are the digital spatial cross section intensity distributions of the images shown in (**a**), (**b**) and (**c**), respectively.

when the polarization direction of P_2 in front of the CCD camera is parallel ($\parallel$) to that of the illuminating beam. Figure 6(b) displays the perpendicular image recorded when the polarization direction of P_2 is perpendicular ($\perp$) to that of the illuminating beam. Figure 6(c) displays the difference image obtained by subtracting the perpendicular image [Fig. 6(b)] from the parallel image [Fig. 6(a)]. Figures 6(d), (e), and (f) show the digital spatial cross section intensity distributions of the images shown in Figures 6(a), (b), and (c), respectively.

The salient features of these images and their intensity distributions are: (i) The peak intensity of the cancerous tissue of the parallel image shown in Figure 6(d) is slightly higher than that of perpendicular one shown in Figure 6(e). This difference can be explained because the light reaching the CCD camera is still partially polarized (16). The preferred polarization direction is parallel to that of illuminating beam, and (ii) the relative brightness of the stained cancerous piece in comparison with the stained normal piece for the polarization difference image shown in Figure 6(c) is obviously higher than those of the conventional polarization images shown in Figures 6(a) and 6(b). To quantitatively describe the improvement of the relative brightness of the dyed cancerous area to the dyed normal tissue area for the polarization difference image, the contrasts (C) of the cancerous tissue area relative to the normal tissue area for all of the polarization and difference images were calculated. C is defined as:

$$C = (I_c - I_n) / (I_c + I_n) \quad [1]$$

where I_c and I_n are the local maximum values of the cancerous and normal tissue area, respectively. Using the digital data shown in Figures 6(d), (e), and (f), the contrasts for these parallel, perpendicular, and polarization difference images are calculated to be 0.28, 0.26, and 0.45, respective-

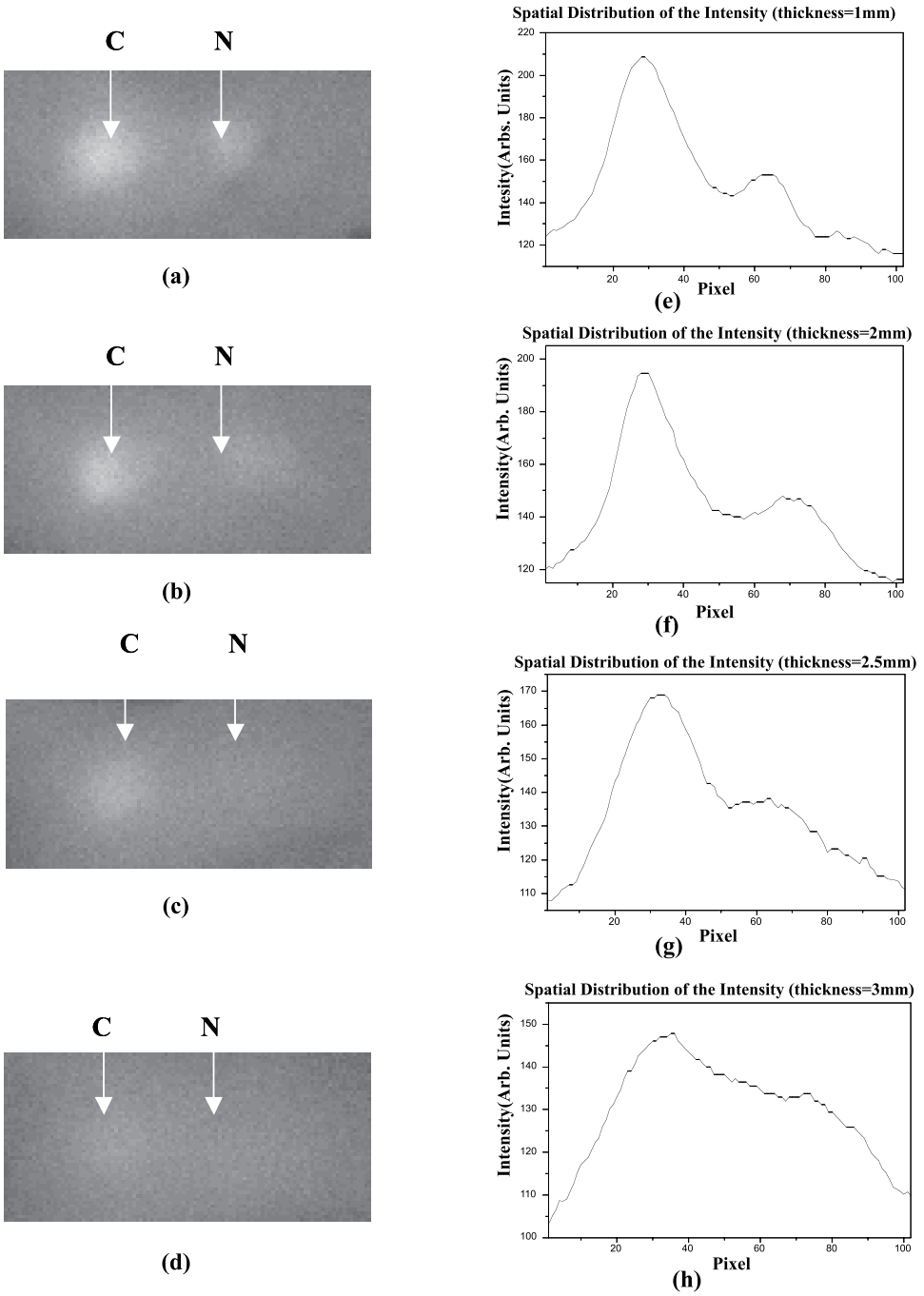

Figure 7: Depth-dependence of contrast agent emission images of a prostate cancer-and-normal tissue sample recorded at λ_{pump}=750nm and $\lambda_{detection}$=850nm with a perpendicular polarization configuration for depths of (**a**) ~1mm, (**b**) ~2mm, (**c**) ~2.5mm, and (**d**) ~3 mm from the surface of the host normal tissue. (**e**), (**f**), (**g**), and (**h**) are the cross section intensity distributions of the images of (**a**), (**b**), (**c**), and (**d**) at the same row crossing the areas of the stained cancer (C) and normal (N) tissues. (**a**) to (**c**) and (**e**) to (**g**) clearly show that the intensity in the cancerous tissue area is much brighter than that of the normal tissue area. From (**d**) and (**g**), for a depth of ~3mm, although the image is blurred, the cancerous region can still be distinguished.

ly. These results indicate that Cybesin has a polarization preservation property similar to ICG, and the polarization difference image shown in Figure 6(c) has a better image contrast than that of the individual polarization images.

The image of the Cybesin dyed prostate cancerous and normal tissues hidden inside the host tissue is formed by photons emitted from Cybesin that have undergone coherent scattering (ballistic photon), less scattering (snake photon), and multiple scattering (diffusive photon) (17). Since most of the photons emitted by the contrast agent undergo multiple scattering, only small percentage of the photons retain their polarization information while they propagate in tissue, the intensities of the two image components $I_{\parallel}$ and $I_{\perp}$ have only small difference. When the two image components are subtracted ($I_{\parallel} - I_{\perp}$), the strong diffusive image component is canceled out. Therefore the contrast of the polarization difference image is much better than that of each individual polarization image.

We also investigated the depth dependence of images at λ_{pump}=750 nm and $\lambda_{detection}$=850 nm using the sandwiched structure of the prostate tissue samples. The thickness of the host normal tissue in front of the stained cancerous and normal tissue pieces was varied up to 3 mm. In order to compare images of objects at different depths in the same polarization configuration, perpendicular imaging was measured. Figures 7(a) to (d) show the backscattering contrast agent emission images of the pair of stained cancerous-normal tissue pieces hidden by depths of ~1 mm, ~2 mm, ~2.5 mm, and ~3 mm, respectively. Figures 7(e), (f), (g), and (h) show the spatial cross section intensity distributions of the images of Figures 7(a), (b), (c), and (d), respectively. The results show that the intensity difference between normal and cancerous tissue can be clearly distinguished up to a depth of ~2.5 mm. At a depth of ~3 mm, the image is blurred, but the intensities of cancerous tissue are still stronger than that of normal tissue.

Conclusion

Spectral measurements of a receptor-target contrast agent, Cybesin, and an optical imaging study was performed for human prostate cancerous and normal tissue stained with Cybesin. The experimental results show that prostate cancerous tissue takes up more Cybesin than normal tissue, and Cybesin can be used as a marker of a cancerous region. In addition, Cybesin is a sound contrast agent because its absorption and fluorescence spectra are in the NIR "tissue optical window". The fluorescence-polarization-difference-imaging (FPDI) technique was used to enhance the contrast between cancerous and normal tissue area. The depth dependence of polarization imaging was investigated. With optimum conditions using λ_{pump}=750 nm and $\lambda_{detection}$=850 nm, the cancerous prostate tissue can be distinguished at a depth of ~3 mm using this contrast agent even for weak illumination of ~50 $\mu W/cm^2$.

Acknowledgement

This research is supported by U. S. Army Medical Research and Material Command grant numbered DAMD17-01-1-0084 (CUNY RF 47462-00-01). The authors acknowledge the help of HUMC and NDRI for providing normal and cancer prostate tissue samples for the measurements, in particular, to Ms. Alexandra T. Sawczuk, RN at HUMC for her arrangement of prostate tissue samples.

References

1. A. Abrahamsson and D. Bostwick. *The Biological Nature of Prostate Cancer – A Basis for New Treatment Approaches*. http://www.urologi.org/sota/STA026/sta26app.pdf.
2. D. A. Benaron. The Future of Cancer Imaging. *Cancer Metastasis Rev. 21*, 45-78 (2002).
3. V. G. Peters, D. R. Wyman, M. S. Patterson, G. L. Frank. Optical Properties of Normal and Diseased Human Breast Tissues in the Visible and Near Infrared. *Phys. Med. Biol. 35*, 1317-1334 (1990).
4. J. H. Ali, W. B. Wang, M. Zevallos, R. R. Alfano. Near Infrared Spectroscopy and Imaging to Probe Differences in Water Content in Normal and Cancer Human Prostate Tissues. *Technol Cancer Res Treat 3*, 491-497 (2004).
5. J. E. Bugaj, S. Achilefu, R. B. Dorshow, R. Rajagopalan. Novel Fluorescent Contrast Agents for Optical Imaging of *In Vivo* Tumor Based on a Receptor-targeted Dye-peptide Conjugate Platform. *J Biomed Opt 6*, 122-133 (2001).
6. L. Kai, B. Riefke, V. Ntziachristos, A. Becker, B. Chance, W. Semmler. Hydrophilic Cyanine Dyes as Contrast Agents for Near-infrared Tumor Imaging: Synthesis, Photophysical Properties, and Spectroscopic *In Vivo* Characterization. *Photochem Photobiol. 72*, 392-398 (2002).
7. W. Wang, J. H. Ali, R. R. Alfano, J. H. Vitenson, J. M. Lombardo. Spectral Polarization Imaging of Human Rectum-Membrane-Prostate Tissues. *IEEE Journal of Selected Topics in Quantum Electronics 9*, 288-293 (2003).
8. D. J. Dean, B. J. Korte. Biomedical Imaging and Bioengineering. *Optics & Photonics News*, October 2003 http://ultra.bu.edu/papers/2003_10_OPN.pdf.
9. G. M. Hale, M. R. Querry. Optical Constants of Water in the 200-nm to 200-Mm Wavelength Region. *Applied Optics 12*, 555-563 (1973).
10. S. J. Goldsmith. Receptor Imaging: Competitive or Complementary to Antibody Imaging. *Semin. Nucl. Med. 27*, 85-93 (1997).
11. S. Achilefu, R. B. Dorshow, J. E. Bugaj, R. Rajagopalan. Novel Receptor-targeted Fluorescence Contrast Agent for *In Vivo* Tumor Imaging. *Investigative Radiology 35*, 479-485 (2000).
12. J. C. Reubi, S. Wenger, J. Schmuckli-Maurer, J.-C. Schaer, M. Gugger. Bombesin Receptor Subtypes in Human Cancers: Detection with the Universal Radioligand (125)I-(D-TYR(6), beta-ALA(11), PHE(13), NLE(14)) bombesin(6-14). *Clin Cancer Res 8*, 1139-1146 (2002).
13. M. Langer, A. G. Beck-Sickinger. Peptides as Carrier for Tumor Diagnosis and Treatment. *Curr Med Chem Anti-Canc Agents 1*, 71-93 (2001).
14. E. D. Gotsis. In Vivo *Proton MR Spectroscopy of Brain Lesions*. Institute of High Medical Technology EUROMEDICA, Advanced Research and Therapeutic Institute ENCEPHALOS. http://users.mland.gr/sgotsis/spectroscopy/mrs.html.

15. W. B. Wang, S. G. Demos, J. Ali, G. Zhang, R. R. Alfano. Visibility Enhancement of Fluorescent Objects Hidden in Animal Tissue Using Spectral Fluorescence Difference Method. *Optical Communications 147*, 11-15 (1998).
16. W. B. Wang, S. G. Demos, J. Ali, R. R. Alfano. Imaging Fluorescence Objects Embedded Inside Animal Tissue Using Polarization Difference Technique. *Optical Communications 142*, 161-166 (1997).
17. L. Wang, P. P. Ho, C. Liu, G. Zhang, R. R. Alfano. Ballistic 2-D Imaging Through Scattering Wall using an Ultrafast Kerr Gate. *Science 253*, 769-771 (1991).

Date Received: January 10, 2005
Date Accepted: July 4, 2005